Disease Models & Mechanisms 4, 43-56 (2011) doi:10.1242/dmm.006262

RESEARCH ARTICLE

Disruption of Mks1 localization to the mother centriole causes cilia defects and developmental malformations in Meckel-Gruber syndrome

Cheng Cui[1], Bishwanath Chatterjee[2], Deanne Francis[2], Qing Yu[2], Jovenal T. SanAgustin[3], Richard Francis[1], Terry Tansey[2], Charisse Henry[2], Baolin Wang[4], Bethan Lemley[2], Gregory J. Pazour[3] and Cecilia W. Lo[1,*]

SUMMARY

Meckel-Gruber syndrome (MKS) is a recessive disorder resulting in multiple birth defects that are associated with mutations affecting ciliogenesis. We recovered a mouse mutant with a mutation in the *Mks1* gene (*Mks1*$^{del64-323}$) that caused a 260-amino-acid deletion spanning nine amino acids in the B9 domain, a protein motif with unknown function conserved in two other basal body proteins. We showed that, in wild-type cells, Mks1 was localized to the mother centriole from which the cilium was generated. However, in mutant *Mks1*$^{del64-323}$ cells, Mks1 was not localized to the centriole, even though it maintained a punctate distribution. Resembling MKS patients, *Mks1* mutants had craniofacial defects, polydactyly, congenital heart defects, polycystic kidneys and randomized left-right patterning. These defects reflected disturbance of functions subserved by motile and non-motile cilia. In the kidney, glomerular and tubule cysts were observed along with short cilia, and cilia were reduced in number to a near-complete loss. Underlying the left-right patterning defects were fewer and shorter nodal cilia, and analysis with fluorescent beads showed no directional flow at the embryonic node. In the cochlea, the stereocilia were mal-patterned, with the kinocilia being abnormally positioned. Together, these defects suggested disruption of planar cell polarity, which is known to regulate node, kidney and cochlea development. In addition, we also showed that Shh signaling was disrupted. Thus, in the neural tube, the floor plate was not specified posteriorly even as expression of the Shh mediator Gli2 increased. By contrast, the Shh signaling domain was expanded in the anterior neural tube and anterior limb bud, consistent with reduced Gli3-repressor (Gli3R) function. The latter probably accounted for the preaxial digit duplication exhibited by the *Mks1*$^{del64-323}$ mutants. Overall, these findings indicate that centriole localization of Mks1 is required for ciliogenesis of motile and non-motile cilia, but not for centriole assembly. On the basis of these results, we hypothesize a role for the B9 domain in mother centriole targeting, a possibility that warrants further future investigations.

INTRODUCTION

Cilia are highly conserved microtubule-based organelles that project from the cell surface and are built on a basal body template derived from the centrosome. Cilia can be motile or non-motile and are found widely, from unicellular organisms such as *Chlamydomonas* to man (Ibanez-Tallon et al., 2003). Cilia assembly is regulated by a conserved mechanism involving transport mediated by intraflagellar transport (IFT) proteins organized in large multiprotein complexes. Cilia serve diverse functions that can entail mediating cell motility and generating fluid flow, or mediating sensory functions such as the detection of light, odorants, protein ligands and other chemicals, as well as mediating mechanosensation for the detection of shear stress, flow and other forces (Eggenschwiler and Anderson, 2007; Gerdes et al., 2009; Satir and Christensen, 2007; Sharma et al., 2008). During embryonic development, motile cilia at the embryonic node generate directional fluid flow, which, together with non-motile sensory cilia at the node periphery, propagates signals that establish the left-right body axis (Hirokawa et al., 2006; McGrath et al., 2003; Okada et al., 2005). Thus, some of the mutations causing left-right patterning defects have been shown to encode proteins that are required for motile function of the cilium, such as left-right dynein expressed in motile cilia of the embryonic node (Supp et al., 1997), or mutations in IFT proteins required for node ciliogenesis, such as Polaris (IFT88) (Murcia et al., 2000) and THM1 (IFT139) (Tran et al., 2008).

Primary cilia also have been shown to have other important functions during embryonic development through their multitude of sensory functions. They mediate the transduction of sonic hedgehog (Shh) signaling by regulating the processing of Gli transcription factors, which are localized in the cilia (Wong and Reiter, 2008). In mammals, Gli2 and Gli3 play essential roles in anterior-posterior patterning of the limb bud, in dorsoventral patterning of the neural tube, and in other developmental processes (Wong and Reiter, 2008). Patched, the Shh receptor, together with Smoothened (Smo) have been shown to regulate proteolytic cleavage of full-length activator Gli3 (Gli3A) into Gli3 repressor (Gli3R) (Haycraft et al., 2005; Hooper and Scott, 2005; McMahon et al., 2003; Rohatgi et al., 2007; Wang et al., 2000). Shh also inhibits

[1]University of Pittsburgh, Department of Developmental Biology, 8111 Rangos Research Center, 530 45th Street, Pittsburgh, PA 15201, USA
[2]National Heart, Lung and Blood Institute, National Institutes of Health, Bethesda, MD 20892, USA
[3]Program in Molecular Medicine, University of Massachusetts Medical School, 373 Plantation Street, Worcester, MA 01605, USA
[4]Department of Genetic Medicine, Weill Medical College of Cornell University, 1300 York Avenue, Room W404, New York, NY 10021, USA
*Author for correspondence (cel36@pitt.edu)

Received 15 June 2010; Accepted 13 September 2010

the processing and degradation of Gli2, with Gli2 being rapidly degraded in the absence of Shh (Pan et al., 2006). The cilium also plays an important role in planar cell polarity (PCP; also referred to as non-canonical Wnt signaling) (Gerdes and Katsanis, 2008) through proteins localized in the cilia, such as Kif3a (Corbit et al., 2008) and inversin (Invs) (Shiba et al., 2009; Simons et al., 2005). Mutations in IFT88 disrupt PCP-regulated patterning of stereocilia bundles in hair cells of the cochlea (Jones et al., 2008). It has also been suggested that polycystic kidney disease, often seen in cilia mutants, might arise from disturbance in the balance between non-canonical (β-catenin independent/PCP) vs canonical (β-catenin dependent) Wnt signaling (Lancaster et al., 2009; McNeill, 2009), with the latter constrained by the cilium (Berbari et al., 2009; Gerdes and Katsanis, 2008).

We recovered a mouse mutant with a constellation of defects that are reminiscent of phenotypes exhibited by patients with Meckel-Gruber syndrome (MKS), an autosomal recessive disorder associated with genes encoding proteins required for ciliogenesis. This mutant was recovered in a large-scale mouse mutagenesis screen for mutations causing congenital heart defects (Shen et al., 2005; Yu et al., 2004). MKS is considered a ciliopathy because five of the six genes associated with MKS are known to be required for ciliogenesis (Baala et al., 2007; Delous et al., 2007; Kyttala et al., 2006; Roume et al., 1998; Smith et al., 2006; Tallila et al., 2008). A pleiotropy of phenotypes observed in MKS were also found in our mouse mutant, including cystic kidneys, polydactyly, cleft lip and/or palate, skeletal anomalies, laterality defects, and congenital heart malformations (Braithwaite and Economides, 1995; Fraser and Lytwyn, 1981; Ickowicz et al., 2006; Mecke and Passarge, 1971; Nyberg et al., 1990; Salonen, 1984; Salonen and Paavola, 1998; Sepulveda et al., 1997). Our mutant was found to have a mutation in *Mks1*, an MKS gene encoding a protein that is localized in the centrosome and basal body (Dawe et al., 2007; Gorden et al., 2008; Tallila et al., 2008). The mutation encompasses a portion of the highly conserved B9 domain found in two other basal body proteins (Town et al., 2008; Williams et al., 2008). Analysis using antibodies to Mks1 showed that, in wild-type cells, Mks1 was localized to the mother centriole from which the cilium was generated (Wheatley, 1982) but, in mutant cells, the truncated Mks1 protein, although still punctate in distribution, was not localized to the centriole. In the mutant, we observed abnormal ciliogenesis in multiple tissues, including in the embryonic node, neural tube, kidney and cochlea of the inner ear. In cochlea, abnormal patterning of the stereocilia was associated with mal-positioning of the kinocilia, indicating perturbation of PCP signaling. We also observed defects in limb and neural tube patterning that were associated with dysregulation of Shh signaling. This was probably brought on by the defects in ciliogenesis. Together, these studies indicate that localization of Mks1 to the centrosome is required for ciliogenesis of both motile and non-motile cilia. Because the protein segment that is deleted in the *Mks1*$^{del64\text{-}323}$ allele includes a portion of the B9 domain, it suggests the possibility that the conserved B9 domain plays a role in the targeting of Mks1 to the mother centriole.

RESULTS

A mouse mutant was recovered that exhibited a wide range of anomalies, including: cleft lip (Fig. 1C); pointy snout (Fig. 1D); eye defects ranging from deeply recessed eyes (enopthalmia), small eyes (microphthalmia) to no eye (anophthalmia) (Fig. 1A,D); polydactyly (Fig. 1A); and congenital heart defects such as transposition of the great arteries (Fig. 1B,E). These anomalies were accompanied by heterotaxy – the randomized left-right positioning of the heart and other visceral organs in the body (Fig. 1B). Analyses of 23 mutants at embryonic day 10.5 (E10.5)-E11.0 showed that 11 had reversed heart looping, and approximately half of the mutants examined at later stages showed dextrocardia, some with a right-sided aortic arch (Fig. 1B,E). We also observed other visceral organ situs defects, including randomized left-right positioning of the stomach (data not shown), abnormal liver situs with some exhibiting symmetric midline liver (Fig. 1F), and polysplenia or asplenia (Fig. 1I and data not shown). In addition, enlargement of the kidneys was observed that, in some cases, was associated with duplex kidneys (Fig. 1J). Histological sections revealed the presence of glomerular cysts and cysts in the kidney tubules (Fig. 2A-D). The latter seem to be derived from the proximal tubules, because only a small number of cysts were positive for the collecting duct and ureteric bud lectin marker *Dolichos biflorus* agglutinin (DBA) (Fig. 2E,F and data not shown).

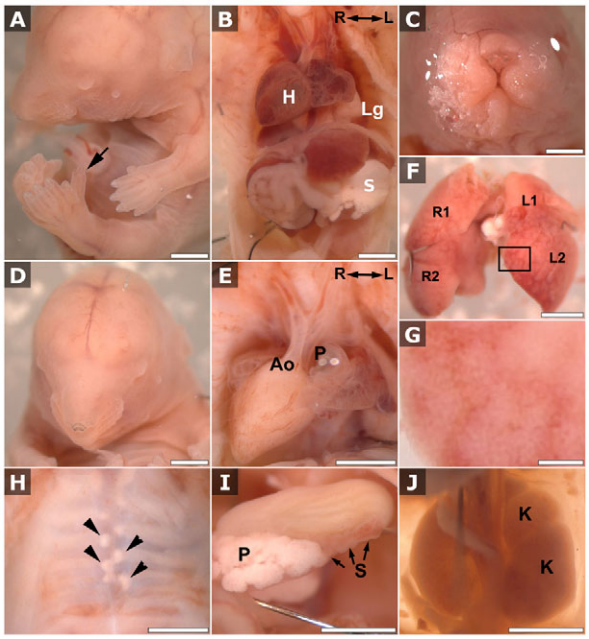

Fig. 1. *Mks1* mutants show multiple anomalies. Spectrum of *Mks1*-mutant phenotypes included preaxial polydactyly (A, arrow) and craniofacial defects – such as pointy snout (A,D), deeply recessed eyes (enopthalmia; A,D) and facial cleft (C). Also observed were complex congenital heart defects – such as transposition of the great arteries (B,E) and randomization of situs as seen in dextrocardia (B,E), symmetric midline liver (F), polysplenia (I) and other visceral organ situs defects. The boxed region in F is enlarged in G to show the cystic appearance of the liver. Skeletal defects were commonly found, such as mal-alignment of the sternal vertebrae (H, arrowheads), and kidney defects were commonly found, including enlarged and duplex kidneys (J). H, heart; Lg, lung; S, stomach; R, right; L, left; Ao, aorta; P (in panel E), pulmonary trunk; P (in panel I), pancreas; S, spleen; K, kidney; L1 and L2, left upper and lower liver lobes, respectively; R1 and R2, right upper and lower liver lobes, respectively. Scale bars in all panels are 2 mm, except in G, where it is 0.25 mm.

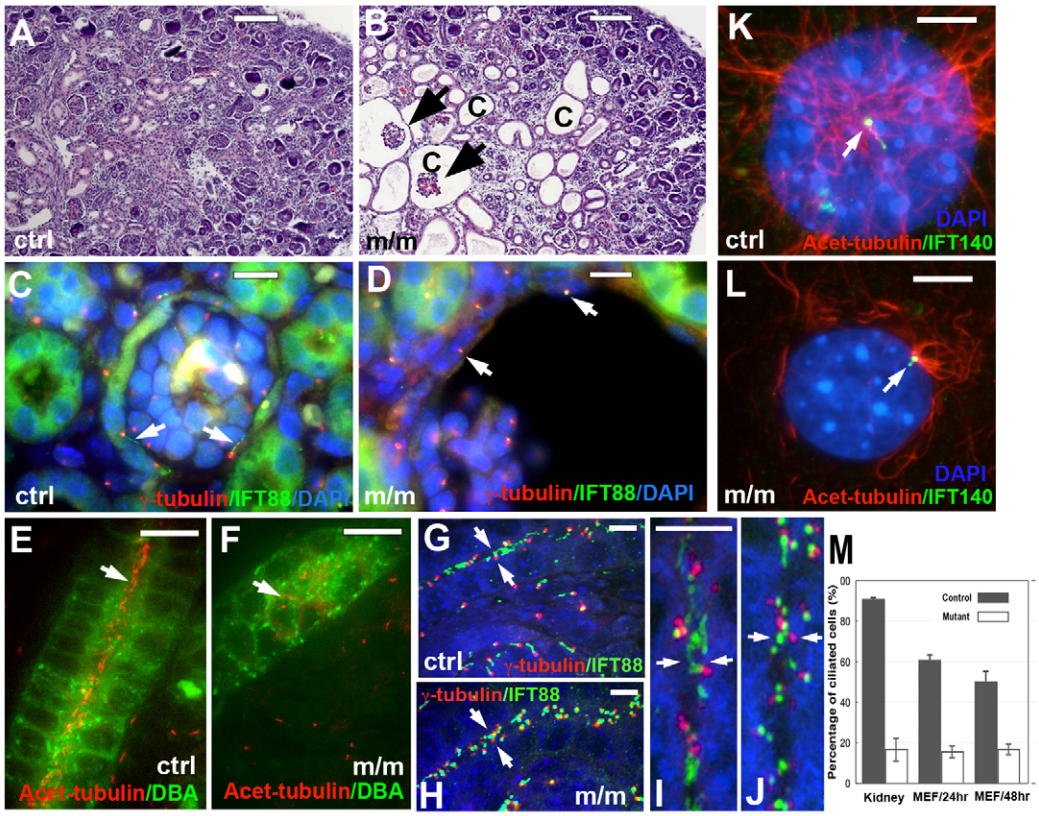

Fig. 2. *Mks1* mutants exhibit kidney cysts and defects in ciliogenesis. (A,B) Hematoxylin and eosin (H&E) staining of paraffin sections from E18.5 wild-type (ctrl; A) and *Mks1* mutant (m/m; B) animals showed the presence of prominent glomerular and tubule cysts ('c') in the mutant animal kidney cortex. Arrows mark glomerular tufts. (C,D) At E18.5, immunostaining with antibody to IFT88 (green) to delineate the cilia (arrows in C,D) showed that cilia were shorter in epithelial cells of mutant glomerular capsule (D) as compared to that of control (C). γ-tubulin (red) was used to delineate the basal body. (E,F) Cilia were less abundant in E17.5 mutant (F) collecting ducts as compared to control (E). The collecting duct was stained with DBA (green) and cilia were stained with anti-acetylated-tubulin antibody (red). Note the presence of cilia (arrow) in the lumen of the control (E) but not the mutant (F) ducts. Images were maximum projections of confocal *z*-stacks. (G-J) Sections of the kidney from control wild-type (G,I) and mutant (H,J) embryos were immunostained with antibodies to γ-tubulin (red) and IFT88 (green). Arrows denote the opposing apical surfaces of the unilaminar kidney tubule epithelia where the centrioles are localized in the control and mutant kidney tubules. The same regions denoted by arrows in G and H are digitally enlarged in I and J. The enlarged panels show that cilia are abundant in the control sample (I), but very few cilia are observed in the mutant kidney tubule (J). (K,L) Cilia (arrow) were shorter in mutant MEFs (L) as compared with control wild-type MEFs (K). The tip and basal body were stained with IFT140 (green) and the ciliary axoneme was stained with anti-acetylated-tubulin antibody (red). (M) Quantitation of cilia observed in the MEF cultures and kidney sections showed significant reductions in the percentage of ciliated cells in the *Mks1* mutant kidney ($P<0.0001$) and mutant MEFs ($P<0.0001$). Scale bars: 100 μm (A,B); 10 μm (C-H); 5 μm (I,K,L).

The appearance of the liver also suggested possible cystic changes (Fig. 1G).

Examination of the mutants further suggested a variety of skeletal anomalies. Mutants exhibited mal-alignment and fissure of the sternal vertebrae (Fig. 1H), and fissure of the manubrium (Fig. 3F). We also found reduced or absent ossification of the vertebral bodies of the cervical and thoracic vertebra (Fig. 3H). In addition, craniofacial defects were observed, including a dome shaped appearance of the skull (Fig. 3B), hypoplastic lower jaw (Fig. 3B) and cleft palate (Fig. 3D). Polydactyly was associated with preaxial digit duplication that included an extra triphalangeal first digit (Fig. 3K,L). This was most often associated with the hindlimb, whereas the forelimb frequently showed a milder phenotype with a broadened thumb (Fig. 1A and Fig. 3I,J). Examination of 34 near-term mutants showed 30 (88%) with polydactyly, of which 28 (82% of all examined) had preaxial digit duplication mainly associated with the hindlimb.

Identification of mutation in *Mks1*

To map the mutation, we intercrossed the mutant that was generated in a C57BL6 background with C3H mice to generate C57BL6:C3H hybrid offspring. The mutant embryos and fetuses obtained from these intercrosses were analyzed by genome scanning using C57BL6/C3H polymorphic DNA markers, and linkage data obtained from ten mutants localized the mutation to mouse chromosome 11. Analysis of an additional 95 mutants using six additional microsatellite DNA markers and 16 SNPs narrowed the interval to a 9.8-Mb region positioned between SNP rs13481117 and rs27099917. This map interval contained 143 genes, including *Mks1*. Reverse transcriptase PCR (RT-PCR) analysis of transcripts derived from genes in the interval in the mutant embryos revealed a deletion of 780 nucleotides in transcripts of *Mks1* that resulted in an in-frame deletion of amino acid residues 64-323 (Fig. 4). In agreement with this finding, sequencing of the genomic DNA from

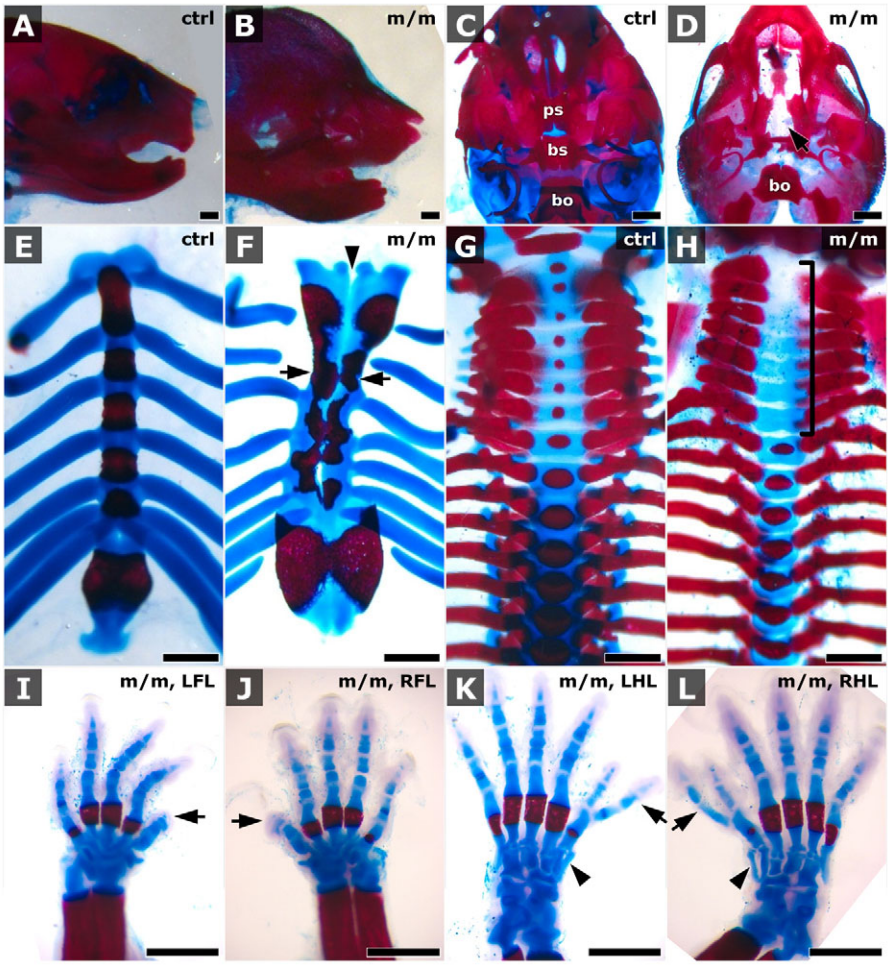

Fig. 3. *Mks1* mutants exhibit skeletal anomalies. (A-H). Skeletal preparations of *Mks1* mutant (m/m; B,D,F,H) and littermate control (ctrl; A,C,E,G) newborn animals showed, in the mutant animal, dome-shaped skull and hypoplastic jaw (B), cleft palate (arrow, D), mal-aligned and split sternal vertebrae (arrows, F), and reduced or absent ossification of the vertebral bodies of the cervical and thoracic vertebrae (bracket, H). Arrowhead in F shows the fissure of sternal vertebrae. (I-L) Skeletal preparations showed *Mks1* mutant animals with preaxial digit duplication with a triphalangeal first digit in the hind limb (arrows in K and L) and broadened thumbs in the forelimb (arrows in I and J), as well as extra carpal bone (arrowheads in K and L). ps, presphenoid; bs, basisphenoid; bo, basioccipital; LFL, left forelimb; RFL, right forelimb; LHL, left hindlimb; RHL, right hindlimb. Scale bars: 1 mm.

the mutant revealed a corresponding deletion of 5226 bases that spanned intron 2 to intron 10 of *Mks1* (Fig. 4). Subsequent genotyping analysis showed that all offspring exhibiting the mutant phenotype were homozygous for the $Mks1^{del64\text{-}323}$ mutation, whereas all viable adult animals were wild-type or heterozygous ($Mks1^{del64\text{-}323}$/+).

Abnormal protein localization in *Mks1* mutant MEFs

To examine the functionality of the mutant Mks1 protein, we generated an antibody to Mks1 by using an epitope outside of the deleted domain, a region that is completely conserved between mouse and human MKS1 (see Methods). In addition, we generated expression constructs encoding wild-type or mutant Mks1 protein fused in frame at the N-terminus with a FLAG tag, and these were transfected into human HEK293 cells. Analysis of the transfected cells by two-color western blots showed dual detection of the expected FLAG-tagged 67-kD wild-type (upper arrow in Fig. 4C) and 37-kD mutant (arrowhead in Fig. 4C) Mks1 fusion protein bands by anti-FLAG (green) and anti-Mks1 (red) antibodies. In addition, the endogenous 64-kD Mks1 protein band was also observed in the nontransfected and transfected cells (lower arrow in Fig. 4C). Additional bands observed with the Mks1 and FLAG antibodies were nonspecific, because they were also found in the nontransfected cells.

Double immunostaining of the transfected HEK293 cells showed that the FLAG and Mks1 protein epitopes were colocalized to the centrosome in cells expressing the wild-type FLAG-tagged Mks1 protein. By contrast, in cells expressing the FLAG-tagged mutant Mks1 protein, no FLAG tag was observed in the centrosome, indicating that the mutant protein could not be incorporated into centrosomes (data not shown). Similar results were obtained with further analysis of mouse embryonic fibroblasts (MEFs) derived from wild-type and *Mks1*-mutant embryos. Wild-type MEFs that were double immunostained with the anti-Mks1 antibody and antibody to γ-tubulin showed colocalization of Mks1 and γ-tubulin in punctate dots corresponding to centrosomes in 30% of the cells (Fig. 4D). In the *Mks1*-mutant MEFs, although Mks1 was also observed in punctate dots, these were not colocalized with the γ-tubulin-containing centrosomes (Fig. 4E). Together, these findings show that the mutant Mks1 protein cannot be assembled into centrosomes. Consistent with this, transfection of a full-length Mks1-GFP construct showed centrosome localization (Fig. 4F), but this was not observed with expression of a full-length mutant-Mks1–GFP construct (Fig. 4G).

Developmental anomalies associated with defects in ciliogenesis

To examine the role of Mks1 in ciliogenesis, we examined cilia outgrowth in wild-type and *Mks1*-mutant MEFs using antibodies

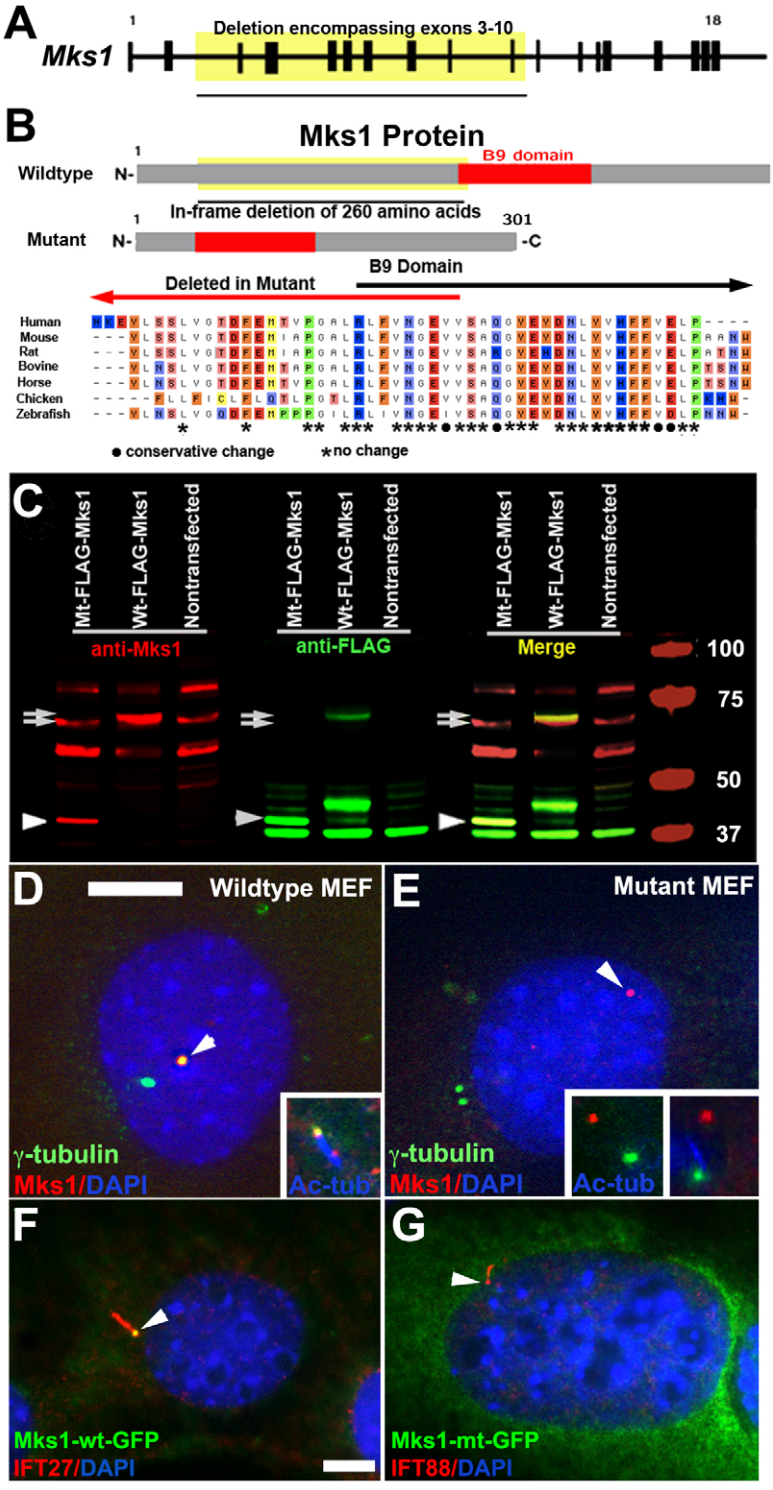

Fig. 4. Recovery and analysis of an in-frame deletion mutation of *Mks1*. (A) Schematic of the mouse *Mks1* gene, containing 18 exons, with the deleted genomic region highlighted, which corresponds to 5226 bases spanning exons 3-10. The sequencing trace file (not shown) from sequencing the genomic DNA (left trace file) showed that the sequence from intron 2 is contiguous with intron 10, whereas sequencing of the cDNA (right trace file) showed that the sequence from exon 2 is contiguous with exon 11 (mRNA). (B) Diagram showing the structure of wild-type and mutant Mks1 protein, with the region deleted delineated in yellow highlight. The in-frame deletion generates a truncated Mks1 protein with amino acid residues 64-323 deleted. (C) Western immunoblotting shows specificity of the anti-Mks1 antibody. Cell lysates from stably transfected HEK293 cells expressing N-terminal FLAG-tagged wild-type (Wt) or mutant (Mt) Mks1 protein were analyzed by western immunoblotting using two-color westerns with an anti-FLAG (green) and anti-Mks1 (red) antibodies. Cells expressing the FLAG-tagged wild-type Mks1 protein exhibited a 67-kD band (upper arrow) that was detected by both the anti-FLAG (green) and -Mks1 (red) antibodies (see merged panel), whereas a slightly smaller 64-kD band (lower arrow), the size expected for endogenous wild-type Mks1, was detected by anti-Mks1 antibody in nontransfected and transfected cells. In cells transfected with the mutant FLAG-tagged Mks1 construct, in addition to the expected 64-kD band, a lower 34-kD band was detected by both the anti-Mks1 and -FLAG antibodies (arrowhead), the size expected for the truncated mutant Mks1 protein. (D,E) Immunostaining of wild-type (D) and *Mks1* mutant (E) MEFs with anti-γ-tubulin (green) and -Mks1 (red) antibodies showed that the mutant Mks1 protein is abnormally localized. In wild-type MEFs, γ-tubulin is localized in two punctate dots consistent with centrosome localization, with one showing colocalization with Mks1 (see arrowhead in D). However, in the mutant MEFs, Mks1 staining (red), although still localized in a punctate dot, is not colocalized with the γ-tubulin (green)-containing centrosomes (E, arrowhead). The inset in D of a wild-type MEF shows that Mks1 (red) is colocalized with γ-tubulin (green) and is in the centriole associated with the primary cilium, which is delineated with anti-acetylated-tubulin antibody staining (blue). By contrast, in the mutant MEFs, Mks1 (red) is not colocalized with γ-tubulin (green), either when the cilium is absent (left inset in E), or in rare instances where a cilium (blue)-like projection is observed (right inset in E). Panels D and E are at the same scale; scale bar in D: 5 μm. (F,G) IMCD kidney cells transfected with plasmids encoding GFP-tagged wild-type Mks1 (F) and mutant Mks1 (G) proteins. GFP-tagged wild-type Mks1 protein showed localization at the base of the cilium (F), but this was not observed with GFP-tagged mutant Mks1 protein (G). The cilia (arrowheads) were delineated with anti-IFT88 (G) or -IFT27 (F) antibodies. Panels F and G are at the same magnification; the scale bar in panel F: 5 μm.

to γ-tubulin and acetylated tubulin to delineate the centriole and cilium, respectively (Fig. 2K,L). Quantitative analysis showed that, in wild-type or heterozygous MEFs, 50-60% of the cells were ciliated, but less than 20% of the homozygous mutant MEFs had cilia (Fig. 2M). To further evaluate ciliogenesis in cells and tissues of the mutant embryos, we used scanning electron microscopy (EM) and light microscopy to examine cilia in the embryonic node, developing kidney, neural tube, cochlea and trachea.

Cilia defects in the embryonic node

Scanning EM analysis of E7.5-E8.0 embryos showed cuboidal epithelial cell morphology in the embryonic node of wild-type or

heterozygous mutant embryos (Fig. 5A), whereas, in the homozygous mutant embryos (n=4), the node had a flattened epithelial morphology (Fig. 5B). In wild-type or heterozygous embryos, most cells in the embryonic node exhibited a single cilium that projected posteriorly. By contrast, in homozygous *Mks1*-mutant embryos, only a few randomly oriented abnormal short cilia-like projections were observed in a few cells in the node (arrows in Fig. 5D-F), but these were not immunostained by an anti-acetylated-tubulin antibody (data not shown). Videomicroscopy also showed no ciliary motion and fluorescent beads placed over the node showed no net nodal flow (see supplementary material Movies 1 and 2).

Cilia defects in the kidney

To evaluate ciliogenesis in the kidney of E18.5 embryos, paraffin sections of the fetal tissue samples were immunostained with anti-IFT88 and anti-acetylated-tubulin antibodies. Cilia were readily found in Bowman's capsule and the glomerulus, as well as in the epithelia of the collecting ducts (Fig. 2C,E). By contrast, in *Mks1*-mutant embryos, very few cilia were observed and, even when present, were shorter than those seen in wild-type or heterozygous embryos (Fig. 2D,F vs 2C,E). Quantitation of the number of ciliated cells in the collecting ducts showed that more than 90% were ciliated in wild-type embryos, but less than 20% were ciliated in mutant embryos (Fig. 2M). Immunostaining with antibodies to γ-tubulin and IFT88 showed that the centrioles were apically localized in the epithelia of the mutant kidney tubules, as observed in the control (wild-type or heterozygous) kidney epithelia (Fig. 2G-J; arrows denote apical surface of opposing unilaminar epithelia in kidney tubule, with enlargement shown in panels I,J).

Cilia defects in the neural tube

Scanning EM analysis of the neural tube showed abundant cilia in the ventral groove encompassing the presumptive floor plate and also in regions dorsolateral to the floor plate. Cilia in the floor plate were generally longer than those on the lateral wall (Fig. 6B vs 6D). In the *Mks1*-mutant embryos, we found fewer cilia, both in the ventral groove (Fig. 6C) and along the lateral wall (Fig. 6E). Often it was difficult to determine whether membrane projections observed in the neural tube of mutant embryos were indeed cilia (Fig. 6E).

Kinocilia and stereocilia patterning defects in the cochlea

We examined the formation of specialized cilia in the developing cochlea that are known as the kinocilia. Kinocilia play a crucial role in the patterning of actin-based microvilli, which are referred to as stereocilia, a process that is regulated by cilia-transduced PCP signaling (Jones et al., 2008; Kelly and Chen, 2007). In the cochlea, there are normally three outer rows [outer hair cells (OHCs)] and one inner row [inner hair cells (IHCs)] of hair cells, and, in each hair cell, a kinocilium is positioned at the tip of the 'chevron'-shaped stereocilia bundles (Fig. 7A). In the *Mks1*-mutant cochlea, although the kinocilia were present and seemed to be of normal length and morphology, they were often misplaced relative to the stereocilia bundles (Fig. 7D-F). Thus, sometimes they were found adjacent to or within the stereocilia bundles (Fig. 7D), displaced to one side of the stereocilia bundles (Fig. 7F) or encircled by a stereocilia bundle ring (Fig. 7E).

Trachea epithelial cells are ciliated and motile

The respiratory epithelia in the trachea have multiciliated cells with motile cilia that move in rapid synchrony to clear mucus, bacteria and other foreign matter from the airway. These ciliated cells emerge during late fetal development, and are sparse near term but rapidly increase in number with postnatal development (Francis et al., 2009). Examination of near-term wild-type and *Mks1*-mutant fetuses showed that both had multiciliated cells with motile cilia (see supplementary material Movie 3). There was no detectable difference in the ciliary motion observed in the wild-type vs mutant airway epithelia. These findings suggest that *Mks1* is dispensable for ciliogenesis in the airway epithelia.

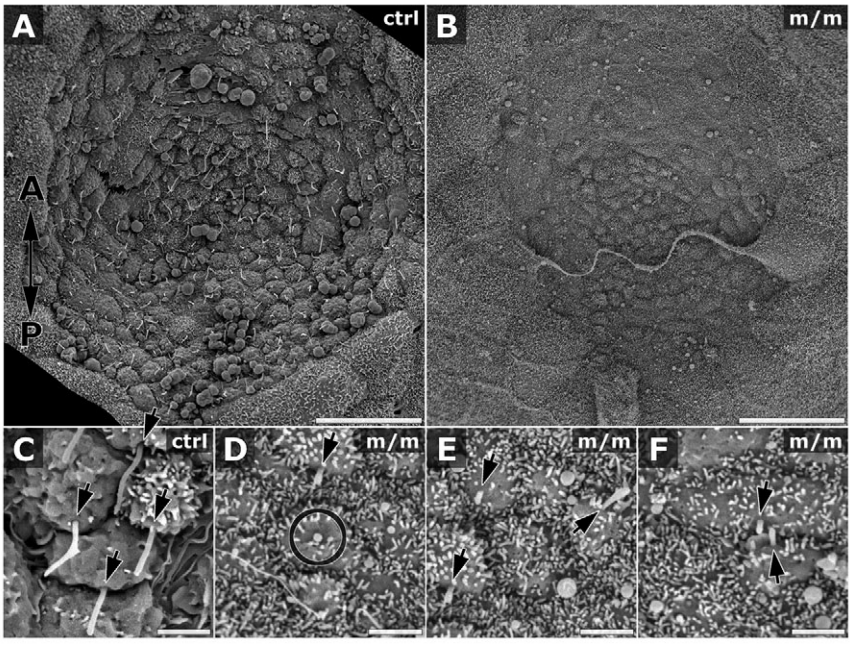

Fig. 5. Scanning EM images of embryonic node cilia. Whereas the control (ctrl) embryo exhibited cells with cuboidal shaped (A), the mutant (m/m) node exhibited flat epithelial cell morphology (B). Cilia in the control node projected posteriorly (arrows in C) from the posterior hemisphere of nodal cells but, in *Mks1*-mutant embryos, node cells exhibited mostly amorphous protrusions (circle in D) and, when cilia were observed, they were shorter (10-30% of length in control node) and were randomly oriented (arrowheads in D-F). Arrows in C-F point to the roots of cilia, with the arrow aligned with the direction of cilium-projection. The two-ended arrow in panel A indicates the orientation of images in all panels, with posterior end of the embryonic node pointing down and anterior end pointing up. Scale bars: 20 μm (A,B); 2 μm (C-F).

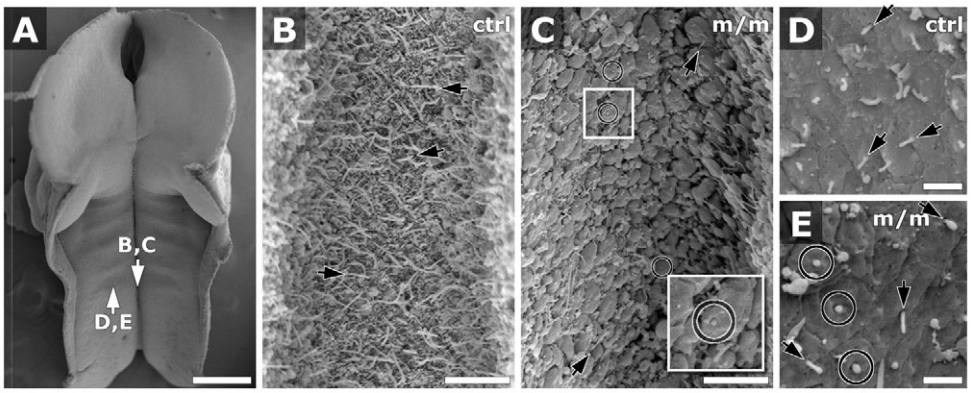

Fig. 6. Scanning EM shows cilia abnormalities in the neural tube. Scanning EM of an E10.5 embryo (A) was used to visualize cilia in the neuroepithelium. Magnified views (B-E) show cilia in the ventral groove (B,C) and lateral wall (D,E) of the hindbrain. Cilia in the ventral groove in control (ctrl) embryos were longer (2-3 µm; B, arrows) than those on the lateral wall (0.5-1.0 µm; D, arrows). In the *Mks1*-mutant (m/m) embryo (C,E), most cells showed only small globular protrusions (circles; see inset in C showing 200% enlargement of boxed region). Nevertheless, fewer cilia were observed in the mutant embryo (C, top-right arrow; E, top-right arrow) than in the control embryo (arrows in B,D). (D,E) Direction of arrows denotes orientation of cilia projection. Scale bars: 400 µm (A); 5 µm (B,C); 2 µm (D,E).

Defects in Shh signaling and abnormalities in dorsoventral patterning of the neural tube

We further examined dorsoventral patterning of the neural tube in *Mks1* mutants because this has been well described to be regulated by cilia-transduced Shh signaling. Sections were obtained from E10.5 *Mks1* mutant and control embryos to examine neural tube patterning anteriorly at the region between the forelimb and hindlimb (Fig. 8A-G) and posteriorly at the level of the hindlimb (Fig. 8H-N). Shh was detected in the notochord, both anteriorly and posteriorly, but expression levels were greatly diminished (Fig. 8A,H). Shh expression was retained in the presumptive floor plate anteriorly but at diminished levels, whereas, posteriorly, Shh was not detected in the ventral neural tube. These observations suggest that the floor plate was present anteriorly but absent posteriorly. We note that, posteriorly, the ventral neural tube had an abnormal thickened morphology, not typical of the floor plate (Fig. 8H,I). Consistent with loss of the floor plate posteriorly, FoxA2, another floor plate marker, was expressed anteriorly (Fig. 8B) but was entirely absent posteriorly (Fig. 8I). In addition, expression of Nkx2.2, a marker of V3 interneurons in the ventral neural tube, was disrupted posteriorly but not anteriorly (Fig. 8M,F). Overall, these findings suggest that the high-level Shh signaling required for floor plate specification was disrupted in the posterior neural tube of *Mks1* mutants, whereas, anteriorly, Shh signaling persisted, but at lower level, as indicated by the reduced expression of FoxA2 and Shh in the presumptive floor plate. In addition, the dorsal limits of Olig2-expressing (Fig. 8C,J) and Nkx6.1-expressing (Fig. 8D,K) domains and the ventral limit of the Pax7-expressing (Fig. 8G,N) domain shifted to more-dorsal positions in the anterior but not posterior neural tube, indicating the dorsal expansion of low-level Shh signaling anteriorly (Fig. 8C,D). Western immunoblotting of the neural tube spanning the region between the forelimb and

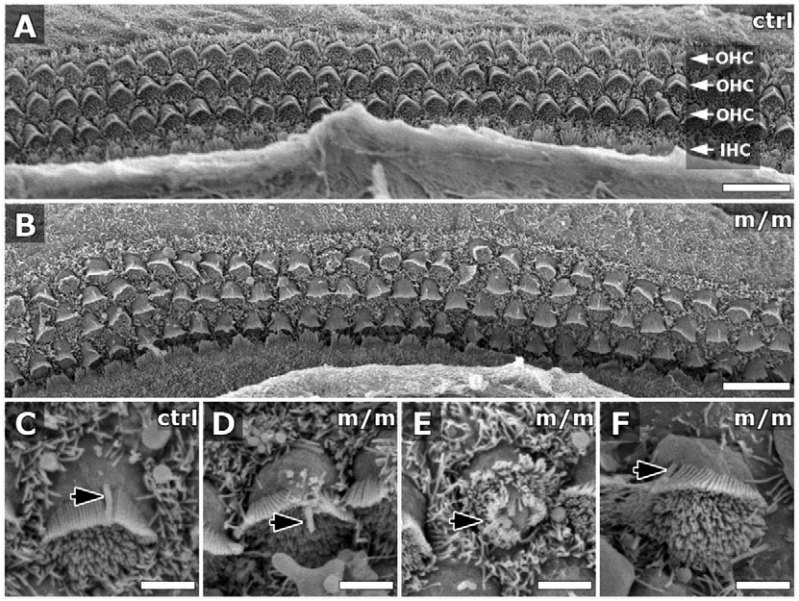

Fig. 7. Scanning EM shows defects in patterning of cochlear hair cells in *Mks1* mutants. In newborn wild-type (ctrl) cochlea (A), three rows of OHCs were aligned in parallel rows (arrows in A) but, in the *Mks1* mutant animal (m/m; B), some OHCs were mal-positioned, with abnormal orientation of the stereocilia hair bundles. Higher magnification (C-F) showed that kinocilia (black arrows) in mutant hair cells (D-F) were of normal length compared to controls (C), but they were abnormally localized relative to the stereocilia hair bundles.

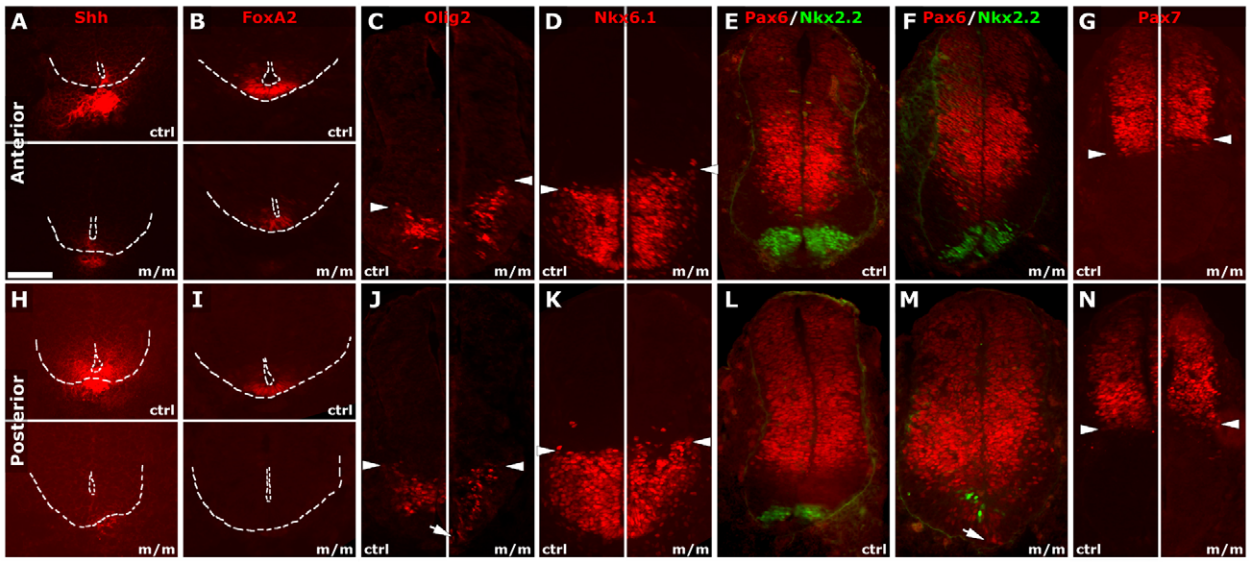

Fig. 8. Dorsoventral neural tube patterning defects in *Mks1* mutants. Expression of dorsoventral markers in the neural tube anteriorly at the level between the forelimb and hindlimb (A-G) and posteriorly, at the hindlimb level (H-N), were examined by immunohistochemistry of wild-type (ctrl) and *Mks1*-mutant (m/m) embryo cryosections. Note that the figure includes panels with top-bottom and left-right side-by-side placement of control and mutant embryo sections. (A-G) Anteriorly, the floor plate in *Mks1* mutants was specified (A,B), even though Shh expression was markedly reduced compared with control (A,B). Thus, the floor plate marker FoxA2 (B) and also Nkx2.2 (E) were expressed ventrally, but at lower levels. As observed in the control, expression of Olig2 (C) and Pax6 (E) in the mutant embryo was separated by the floor plate. The dorsal limit of Olig2 (C) and Nkx6.1 (D) and ventral limit of Pax7 (G) were observed to shift dorsally. (H-N) At the posterior level, the floor plate was not specified and ventral neural tube exhibited an abnormal thickened morphology in mutants. Thus, neither Shh (H) nor FoxA2 (I) expression was detected in the mutants, and only a few cells expressed Nkx2.2 (M). Olig2 (J) and Pax6 (M) expanded ventrally (arrows in J and M) in mutants, whereas the dorsal limits of Olig2 (J), Nkx6.1 (K) and the ventral limit of Pax7 (N) were at almost the same level as in control (denoted by arrowhead in J, K, N). (A,B,H,I) The apical and basal surfaces of the ventral neural tube are delineated with white dashed lines. Arrowheads indicate the dorsal or ventral limits of expression of the respective markers. Scale bar: 50 μm.

hindlimb showed an increase in full-length Gli3 (Gli3-FL) but no change in Gli3R level (supplementary material Fig. S1B,D,E). We also observed an increase in full-length Gli2 protein expression level (supplementary material Fig. S1C,E).

Defects in Shh signaling in the limb and abnormal digit patterning

The finding of polydactyly in the *Mks1* mutants suggested a defect in Shh signaling, because Shh is required for normal anterior-posterior patterning of the limb bud. In situ hybridization analysis showed that, in E10.0-E10.5 limb buds, *Shh*, *Gli3* and *dHand* expressions were unchanged (Fig. 9B-D vs 9G-I), but *Gli1* and *Ptc1* expressions were reduced (Fig. 9A,F and supplementary material Fig. S2C,D). At E11.0, a reduction in *Ptc1* expression in the posterior limb bud was accompanied by ectopic *Ptc1* expression in the anterior limb bud (Fig. 9E,J). This was accompanied by an anterior expansion in the expression domains of *Fgf8* (Fig. 9K,P), *Fgf4* (Fig. 9L,Q) and gremlin (Fig. 9M,R). At E12.5, the *Sox9* expression domain was broadened anteriorly in the presumptive first digit of the forelimb, and in the anterior protrusion of the hindlimb bud (Fig. 9S,T vs 9N,O). Overall, these findings indicated ectopic activation of *Shh* signaling in the anterior limb bud. Using western immunoblot analysis, we examined Gli3 expression levels in the limb buds. Left limb buds were bisected into anterior and posterior halves, whereas the right limb buds were harvested whole. This analysis revealed a reduction in the Gli3R:Gli3-FL ratio in the anterior but not posterior halves of the fore- and hindlimb buds compared with controls. A reduction in the Gli3R:Gli3-FL ratio was also detected in the whole hindlimb bud but not forelimb bud compared with controls (supplementary material Fig. S1A,B). These results suggest that the preaxial polydactyly typically observed in the *Mks1* mutant results from a relative decrease in Gli3R level in the anterior limb bud brought on by the ectopic activation of Shh.

DISCUSSION

We recovered a mouse model of MKS with a recessive mutation in the *Mks1* gene. We showed that the mutation is an in-frame deletion spanning amino acid residues 64-323 of Mks1 (*Mks1*$^{del64\text{-}323}$). Immunostaining showed that the wild-type and mutant Mks1 proteins were both distributed in punctate dots, but only the wild-type Mks1 protein was localized in the centriole. Analysis of wild-type MEFs showed that the endogenous Mks1 protein was localized to the mother centriole associated with the primary cilia, whereas, in the *Mks1* mutant MEFs, there was a defect in ciliogenesis that was associated with failure of the Mks1 protein to localize to the centriole. These observations suggest that the mutant Mks1$^{del64\text{-}323}$ protein disrupts ciliogenesis by its failure to be incorporated into the mother centriole.

Our homozygous *Mks1* mutants exhibited a wide range of birth defects that are similar to those observed in MKS patients, including cystic kidneys, polydactyly, and craniofacial defects with cleft palate, as well as heterotaxy and congenital heart defects (Braithwaite and Economides, 1995; Fraser and Lytwyn, 1981; Ickowicz et al., 2006; Katsanis, 2006; Mecke and Passarge, 1971;

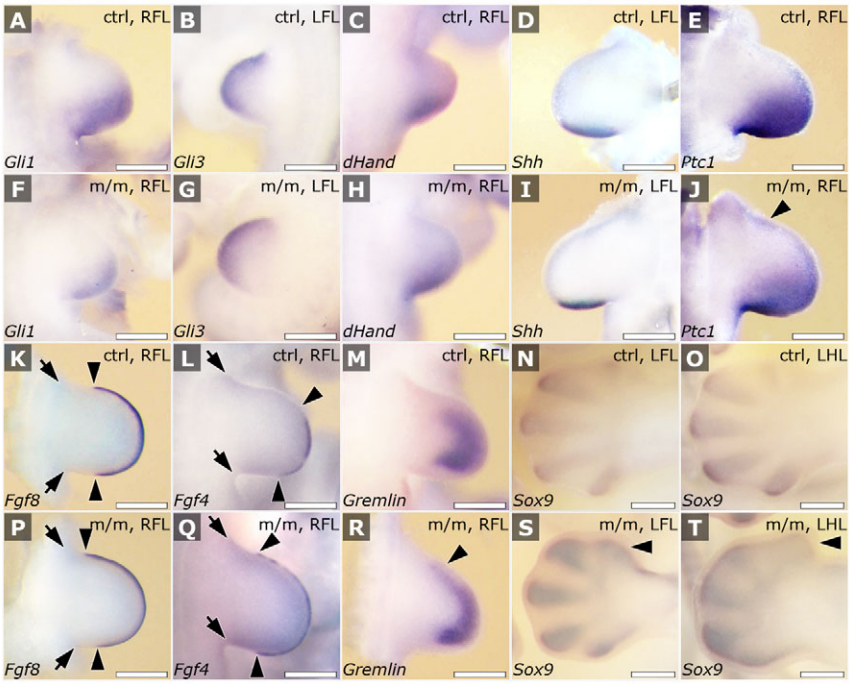

Fig. 9. Analysis of limb patterning defects by in-situ hybridization analysis. *Shh*, *Gli3* and *dHand* transcripts showed normal distribution in E10.25 (*Gli3*, *dHand*; B,C,G,H) and E10.5 (*Shh*; D,I) mutant (m/m) limb buds. *Gli1* (A,F) and *Ptc1* expression were lower at E10.5 (supplementary material Fig. S2) in mutant compared with control embryos. By E10.75-E11.0, *Ptc1* expression recovered, but was still reduced in the posterior limb in the mutants compared with controls (E,J). At this stage, a region of ectopic *Ptc1* expression was observed anteriorly in the mutants (arrowhead, J), and this was accompanied by the anterior expansion of *Fgf8* (K,P) and *Fgf4* (L,Q) (as indicated by paired arrowheads; the arrows indicate the anterior and posterior proximal limits of the limb buds), and gremlin (M,R) expression (top arrowheads). At E12.5, mesenchymal condensations, delineated by *Sox9* expression (N,O,S,T), showed broadening anteriorly in the forelimb, corresponding to the region of the presumptive first digit (arrowhead in S), whereas, in the hindlimb, a more prominent extrusion could be seen, also at the position of the presumptive first digit (arrowhead, T). LFL, left forelimb; RFL, right forelimb; LHL, left hindlimb; RHL, right hindlimb. Scale bars: 400 μm.

Nyberg et al., 1990; Salonen, 1984; Salonen and Paavola, 1998; Sepulveda et al., 1997). These findings indicate that ciliary defects might have broad relevance for a wide variety of birth defects. These birth defects arise from the disruption of normal ciliogenesis, because Mks1 mutants exhibited fewer and shorter cilia in a variety of cells and tissues, including in the embryonic node, neural epithelia, kidney and MEFs.

We note that another Mks1 mouse mutant, kerouac (krc), was recently reported that probably carries a null mutation with complete loss of Mks1 function (Weatherbee et al., 2009). Overall, the phenotype of krc mutants is similar to that of the $Mks1^{del64\text{-}323}$ mutant and is also associated with a reduction in cilia. However, many of the defects observed in the $Mks1^{del64\text{-}323}$ mutants seem to be more severe. For example, whereas krc mutants show polydactyly associated with duplication of the first digit, our mutants show preaxial digit duplication characterized by mirror symmetric duplication of a secondary limb anterior-posterior axis. We also observed more-severe cystic changes in the kidney and, in addition, our mutant exhibited duplex kidneys, which are not observed in the krc mutant. These and other differences would suggest the $Mks1^{del64\text{-}323}$ allele exerts dominant-negative effects related to expression of the abnormal internally deleted Mks1 protein.

Node and cochlea defects suggest Mks1 involvement in the PCP pathway

Our study shows that the left-right patterning defects in the *Mks1* mutant are elicited by defects in the embryonic node, because *Mks1* mutants had little or no cilia in the embryonic node and exhibited no nodal flow. Mutations in a number of other cilia- and/or centrosome-related proteins, such as IFT172, Ftm, OFD-1 and Dnchc2, are also associated with left-right patterning defects (Ferrante et al., 2006; Huangfu and Anderson, 2005; Huangfu et al., 2003; Vierkotten et al., 2007). The cell morphology in the embryonic node in *Mks1* mutants was also altered, and the few cilia observed in the node showed randomized orientation. These findings suggest a disruption in PCP and non-canonical Wnt signaling, because PCP signaling at the embryonic node is required for repositioning of the basal body from a central to posterior position. This redistribution of the basal body generates a posterior tilt to the nodal cilia, and this tilt is crucial for generating nodal flow (Hashimoto et al., 2010). Also consistent with the disruption of PCP signaling is the stereocilia patterning defects in the cochlea, a process that is also regulated by non-canonical Wnt signaling (Kelly and Chen, 2007). Together, these findings suggest that the Mks1 centrosome protein plays an essential role in modulating signaling in the PCP (non-canonical Wnt) pathway.

Cilia defects, kidney cysts and duplex kidneys

Ciliary defects are well known to cause polycystic kidney disease (Pazour et al., 2000) and cysts are observed in *Mks1*-mutant kidneys. Several different models have been proposed to explain how kidney cysts are caused by mutations affecting the cilium. One model suggests that the cilium functions as a mechanosensor to detect flow as a measure of tubule diameter and that cyst formation arises from a failure of the cilia to accurately sense flow (Nauli et al., 2003). An alternative model suggests that cilia balance canonical and non-canonical Wnt signaling in the tubules (Simons et al., 2005), and defects in both of these pathways are observed in *Ift20*-mutant kidneys (Jonassen et al., 2008). The non-canonical Wnt or PCP pathway is thought to be important in orienting cell division along the kidney tubule in order to elongate tubules without increasing diameter (Fischer et al., 2006), whereas the canonical pathway is thought to be important in controlling proliferation (Saadi-Kheddouci et al., 2001). However, unlike what is seen in mice with ciliary defects due to intraflagellar transport mutations (Brown and Murcia, 2003; Jonassen et al., 2008), the cysts in the *Mks1*-

mutant animals formed prenatally. This suggests that Mks1 plays additional roles in preventing cyst formation beyond its role in ciliogenesis.

In addition to kidney cysts, duplex kidneys were also observed in *Mks1*-mutant animals. Duplex kidneys are thought to result from the formation of an ectopic ureteric bud that induces a second kidney that fuses with the normal kidney (Kume et al., 2000). This phenotype might be related to the possible role of Mks1 in regulating tubular branching morphogenesis, because small interfering RNA (siRNA) knockdown of Mks1 was shown to inhibit the formation of branched structures by IMCD-3 cells in three-dimensional cultures (Dawe et al., 2007). Duplex kidneys are also observed as human birth defects, and have been described in mice with defects in forkhead transcription factors (Kume et al., 2000) and bone morphogenic protein 4 (BMP4) signaling (Miyazaki et al., 2000). Because *Bmp4* gene expression is regulated by Shh (Yu et al., 2002), duplex kidney phenotypes also might emerge from the disruption of Shh signaling in *Mks1* mutants. Duplex kidneys have not been described previously in cilia mutants and our finding suggests that this is a new phenotype associated with ciliopathies.

Mks1 is essential for hedgehog signaling

Cilia defects in the *Mks1* mutant are also likely to contribute directly to the abnormal patterning of the neural tube and limb bud through the well-described role of the cilium in the transduction of Shh signaling. Although Shh expression was activated in the notochord in *Mks1* mutants, absence of the floor plate in the posterior neural tube would suggest that Shh signaling was not propagated to the posterior ventral neural tube. This suggested a defect in the Gli2A-mediated high-level Shh signaling required for floor plate specification (Ding et al., 1998; Matise et al., 1998). Nevertheless, because some ventral neuron markers (Olig2 and Nkx6.1) were specified, a low level of Shh signaling must be retained even in the posterior neural tube. By contrast, anteriorly the floor plate was specified and, although expression of floor plate markers was diminished, the dorsal expansion of ventral markers (Olig2 and Nkx6.1) and contraction of a dorsal marker (Pax7) would suggest that the anterior neural tube is ventralized. The mouse cilia mutant *hnn* (Arl13b) also exhibits ventralization of the neural tube, but this was found in conjunction with the complete loss of the floor plate (Caspary et al., 2007).

Because Gli3R activity has been shown to counteract the ventral specification of the neural tube by Shh, ventralization of the anterior neural tube would suggest that Gli3R might be reduced in the *Mks1* mutant. This is also suggested by the finding of ectopic Shh signaling in the anterior limb buds of *Mks1* mutants. Indeed, western immunoblotting of the neural tube and limb buds showed decreased a Gli3R:Gli3-FL ratio. This decrease was due to an increase in Gli3-FL, but no change in Gli3R level. The loss or reduction in floor plate marker expression posteriorly would suggest that Gli2A might be reduced. Our western analysis showed that the protein expression level of full-length Gli2 increased in the *Mks1* mutant; this might serve to compensate for the reduction in Gli2A. Hedgehog perturbations probably also contribute to the craniofacial and skeletal defects in the *Mks1* mutant, which show phenotypic overlap with the Gli2- and Gli3-knockout mice (Mo et al., 1997). Future studies are needed to elucidate whether the disruption in Shh signaling reflects the requirement for Mks1 in ciliogenesis, or whether Mks1 might have a role in signaling.

The role of Mks1 in ciliogenesis

Our observations suggest that defects in ciliogenesis underlie the majority of phenotypes exhibited by the *Mks1* mutant. Previous studies suggested that the Mks1 protein might be required for apical migration of the centriole, which occurs in the earliest stage of ciliogenesis (Dawe et al., 2007). However, we observed apical positioning of the centrioles in the developing kidney tubule of *Mks1*-mutant embryos even though they exhibited very few cilia. Recent studies have identified the requirement for *HYLS-1*, a gene that is associated with hydrolethalus syndrome, in apical targeting and anchoring of the centriole to the membrane (Dammermann et al., 2009). HYLS-1 is said to be the first stably incorporated centriolar protein that is not required for centriole assembly but is required for ciliogenesis. Our studies suggest that Mks1 is another such protein. Thus, in *Mks1*-mutant MEFs and kidney epithelia, γ-tubulin-containing centrioles are formed, but ciliogenesis is severely disrupted. Analysis of the mutant MEFs showed that the mutant Mks1 protein is expressed and shows a punctate distribution, but is not localized to centrioles. On the basis of these findings, we propose that Mks1 is a centriolar protein that is dispensable for centriole assembly but is required for later events in ciliogenesis, post-migration of the centriole to the plasma membrane. This might involve the conserved B9 protein domain that is disrupted by the deletion in the $Mks1^{del64\text{-}323}$ allele – a domain of unknown function conserved in three basal body proteins in the mouse, human and *Caenorhabditis elegans* genome, referred to in *C. elegans* as XBX-7 (MKS1), TZA-1 (B9D2) and TZA-2 (B9D1) (Williams et al., 2008). Studies in *C. elegans* show that all three proteins play a role in ciliogenesis and form a complex that is localized to the base of cilia (Williams et al., 2008). Conditional loss of the mouse ortholog of *tza-1* (*B9D2*; referred to as *stumpy*) causes hydrocephalus and severe polycystic kidney disease (Town et al., 2008; Williams et al., 2008). *stumpy* mutants are cilia deficient, exhibiting occasional shortened or stumpy cilia. Stumpy has been shown to be localized to basal bodies, and coimmunoprecipitates with γ-tubulin (Town et al., 2008). Whereas the wild-type Mks1 protein colocalizes with γ-tubulin, the mutant Mks1 protein does not. However, because the Mks1 protein is normally localized to only the mother centriole from which the primary cilia is generated, the recruitment of Mks1 protein to the centriole cannot be dependent on interactions with γ-tubulin. Because the sequences deleted in the $Mks1^{del64\text{-}323}$ allele include the N-terminus of the B9 domain, further studies are warranted to examine whether the B9 domain plays a role in targeting proteins to the mother centriole (Williams et al., 2008). These findings show the value of mutagenesis screens in allowing the dissection of protein function and suggest that recovery of an allelic series can provide insights for establishing phenotype-genotype correlations.

METHODS

Genome scanning and linkage analysis

The *Mks1* mutant was recovered from a large-scale ethyl-nitrosourea (ENU) mutagenesis screen using fetal echocardiography for cardiovascular phenotyping to recover mutations causing congenital heart disease (Yu et al., 2004; Shen et al., 2005).

Mutations causing a wide range of congenital heart defects were recovered, among which was the *Mks1* mutant (Yu et al., 2004; Shen et al., 2005). All mice were maintained in the NIH Animal Facility, and all experiments involving mice were approved by the NHLBI Institutional Animal Care and Use Committee (IACUC). Genomic DNA from mutant embryos was PCR amplified using dye-labeled primers for 48 B6/C3H polymorphic microsatellite markers spread throughout the mouse genome. The resultant PCR products were separated by capillary electrophoresis on the Avant 3100 Genetic Analyzer (Applied Biosystems, Foster City, CA) and linkage analysis was carried out using recombinant interval haplotype analysis (Neuhaus and Beier, 1998; Yu et al., 2004).

Production of anti-Mks1 antibodies

Polyclonal antibody to Mks1 was raised in chicken by immunization with the synthetic peptide (EAFRRARRRMQEARES) corresponding to amino residues 533-548 at the C-terminus of Mks1 (Aves Labs). The antibody was affinity purified and analyzed by ELISA.

Analysis of Mks1 protein expression

Wild-type or mutant *Mks1* cDNAs were generated by RT-PCR and cloned in-frame 3′ of the FLAG tag in the mammalian expression vector CMV-26. The resulting constructs provided expression of 5′-FLAG-tagged wild-type or mutant Mks1 protein. HEK293 cells (ATCC) were transfected with these constructs using Lipofectamine 2000 and stable transfectants were selected in 500 μg/ml G418 (Cellgro). Transfectant clones were isolated and lysed on ice using RIPA buffer containing protease inhibitor P8320 (Sigma) and analyzed by western immunoblotting after electrophoresis on NuPage 4-12% Bis-Tris gels. Two-color western detection was carried out using primary antibodies consisting of 1:1000 anti-FLAG mouse monoclonal antibody (Sigma) and chicken anti-mouse Mks1 antibody followed by IRDye 800CW donkey anti-mouse IgG (LI-COR) and 700 CW goat anti-chicken (Rockland) (1:15,000) antibodies. After washing, the immunoblots were imaged using a LI-COR Odyssey scanner.

Cell culture, immunocytochemistry and cilia quantification

MEFs were generated from E11.5-E12.5 embryos and early passage cells were serum starved for 24 or 48 hours using DMEM (Invitrogen) supplemented with 0.1-0.5% fetal bovine serum (HyClone) and penicillin/streptomycin. For quantification of cilia, cells were fixed in 4% paraformaldehyde (PFA) for 10 minutes and processed for immunostaining with anti-acetylated-tubulin antibody (Sigma; 1:200). Immunostaining with other antibodies entailed permeabilization of the cells with PHEM/Triton X-100 and fixation in PHEM/2% PFA solution or methanol for 15 minutes at room temperature. Antibodies used included rabbit anti-IFT88 (1:1000), rabbit anti-IFT140 (1:1000) and mouse anti-γ-tubulin (1:500; Sigma).

Sectioning and immunocytochemistry

For cryosectioning, embryos fixed with 4% PFA overnight or freshly harvested were embedded in Tissue-Tek OCT compound (Sakura Finetek, USA) and 14-μm sections were generated. After rinsing with phosphate buffered saline (PBS), sections were blocked with 3% BSA in PBS with Tween-20 (PBST), followed by incubation with primary antibodies, washes, then incubation with secondary antibodies. The antibodies included anti-Shh (1:250), -FoxA2 (1:1000), -Nkx6.1 (1:500), -Pax6 (1:500), -Pax7 (1:1000) and -Olig2 (1:500). For cryosections with 3,3′-diaminobenzidine (DAB) staining, we followed previously described procedures (Ding et al., 2009). Immunostaining of the embryonic node at E7.5-E7.75 and immunostaining of kidney paraffin sections were carried out as previously described (Follit et al., 2008; Jonassen et al., 2008).

Western analysis of Gli protein expression in limb and neural tube tissues

For western blotting, the left fore- and hindlimbs (E10.5; 32-37 somites) were harvested and bisected into anterior and posterior halves, whereas the right fore- and hindlimbs were harvested intact. The remaining embryo body without limbs was harvested as trunk tissue. All tissues were lysed in RIPA buffer with a 1% protease inhibitor cocktail (Sigma), then homogenized and centrifuged to remove residual insoluble material. For Gli3 westerns, the lysates were run on 4-12% polyacrylamide NuPAGE Bis-Tris denaturing gels (Invitrogen) under reducing conditions. For Gli2 westerns, lysates were run on 6% Novex Tris-Glycine gel (Invitrogen). Immunodetection was carried out using the LI-COR Odyssey infrared imaging system and the acquired images were processed with NIH ImageJ software.

In-situ hybridization

Procedures used for whole-mount in-situ hybridization were as described previously (Albrecht, 1997). We followed similar procedures for in-situ hybridization of cryosections, with the aid of in-situ frames (Brinkmann Instruments). Briefly, embedding OCT of cryosections (thickness=14 μm) was rinsed off with PBS, and sections were fixed with 4% PFA and 2% glutaraldehyde in PBS for 5 minutes. After being pre-incubated with hybridization mix, sections were incubated with hybridization mix with digoxin (DIG)-labeled probes overnight at 65°C. The sections were then rinsed with tris-buffered saline with Tween-20 (TBST) and incubated with anti-DIG antibody (1:2000 in blocking solution) overnight at 4°C. Gene expression patterns were revealed with BM purple AP substrate (Roche). DIG-labeled probes were made with DIG RNA labeling reaction mixture (Roche).

Videomicroscopy and scanning electron microscopy

We used previously described procedures to examine nodal cilia motility (Zhang et al., 2009) and beating of cilia on trachea epithelial cells (Francis et al., 2009). For scanning EM, mouse embryos at E7.5-E8.0, or hindbrain or spinal cord tissues at E10.5, were fixed with 2.5% glutaraldehyde in 0.12 M sodium cacodylate buffer, pH 7.4, post-fixed with 1% OsO_4, then dehydrated, critical point dried and mounted with carbon adhesive tape followed by coating with 10-nm gold with an EMS 575X sputter coater. Images were obtained using a Hitachi S3400-N1 scanning electron microscope.

Skeletal staining

For skeletal staining, late-term fetuses or newborn pups were fixed in 10% formalin and eviscerated, followed by dehydration in ethanol, incubation in acetone and staining with 0.15% Alcian Blue, 0.05% Alizarin Red and 5% glacial acetic acid in ethanol. The stained

TRANSLATIONAL IMPACT

Clinical issue

Meckel-Gruber syndrome (MKS) is a lethal recessive disorder with multiple severe birth defects, including polycystic kidneys, polydactyly, cleft lip and palate, skeletal anomalies, laterality defects, and congenital heart malformations. MKS is considered a ciliopathy, because five of the six genes associated with MKS are known to be required for ciliogenesis. However, the exact nature of the ciliary defect in MKS is unclear. Cilia serve diverse biological functions, which include cell motility, generating fluid flow and mediating sensory functions such as detection of light, odorants, protein ligands and other chemicals, as well as regulating mechanosensation in shear stress and flow sensing. During development, motile cilia at the embryonic node generate directional fluid flow, which, together with primary (non-motile) cilia at the node periphery, propagates signals that establish the left-right body axis. Primary cilia also have other important functions during development, such as the transduction of sonic hedgehog (Shh) signaling and planar-cell-polarity (PCP) signaling or non-canonical Wnt signaling. Defects in the diverse functions of motile and non-motile cilia might account for the broad spectrum of developmental malformations observed in MKS patients.

Results

The authors characterize a mouse mutant recovered from an ENU screen that has a constellation of defects that resemble the symptoms observed in MKS patients. In the kidneys of mutant mice, glomerular and tubule cysts are observed, together with short and near complete loss of the cilia. Underlying the left-right patterning defects are fewer and shorter nodal cilia with no directional flow. In the cochlea, the stereocilia are mal-patterned, with the kinocilia abnormally positioned. Together, these defects suggest a disruption in PCP signaling pathways that are known to regulate node, kidney and cochlea development. The authors also show that Shh signaling is disrupted in the neural tube and limb bud of the mutant mice, which underlies preaxial digit duplication. The mutation in these mice maps to *Mks1*, which encodes a protein that localizes to the centrosome (a structure composed of microtubule-based centrioles that is central for ciliogenesis). The mutation disrupts the highly conserved B9 domain of Mks1, which is also found in two other centrosome proteins. The mutant protein no longer localizes to the centrosome, suggesting that the B9 domain plays a role in centrosomal targeting. In *Mks1*-mutant mouse embryonic fibroblasts and kidney epithelia, centrosomes are formed but ciliogenesis is severely disrupted. These findings indicate that the localization of Mks1 to the centrosome is required for ciliogenesis of motile and non-motile cilia, but not for centrosome assembly.

Implications and future directions

This work demonstrates that Mks1 is a centrosomal protein that is required for ciliogenesis, and provides new insights into the molecular events that underlie the wide range of birth defects associated with MKS. Important future studies will include examining the role of the B9 domain in targeting Mks1 to the centrosomes and the role that this plays in ciliogenesis. These findings also emphasize the value of mutagenesis screens for identifying disease-associated genes.

doi:10.1242/dmm.006890

specimen were then rinsed in water and cleared in 20% glycerol with 1% KOH until skeleton and/or cartilage were clearly visible.

ACKNOWLEDGEMENTS

RNA in-situ probe plasmids were generously provided by Lee Niswander (*Fgf4*), Gail Martin (*Fgf8*), Richard M. Harland (gremlin), Marian A. Ros (*dHand*), Richard R. Behringer (*Sox9*) and Chi-chung Hui (*Gli1*). We thank Chi-chung Hui at The Hospital for Sick Children, Toronto, Canada for generously providing reagents and for helpful discussions, Matthew Kelley and Chandrakala Puligilla at NIDCD for help with cochlea dissection, Yingfan Zhang at National Heart, Lung and Blood Institute and Alex Bao at National Cancer Institute for assistance with western blotting, Susan Mackem at NCI for helpful discussions on Gli processing and roles in neural tube and limb patterning, Xiaoyan Ding at Zhongshan Ophthalmic Center, Sun Yat-Sen University, Guangzhou, China for assistance with immunostaining, and Mathew P. Daniels and the NHLBI Electron Microscopy Core Facility for help with scanning electron microscopy. The antibodies (Shh, FoxA2, Pax6, Pax7, Nkx2.2, Nkx6.1) were obtained from the NICHD Developmental Studies Hybridoma Bank, maintained by The University of Iowa, Iowa City, IA. Anti-Olig2 antibody was a kind gift of Bennett Novitch (UCLA), and anti-Gli3 antibody was a kind gift of Susan Mackem (NCI). This work is supported in the Pazour laboratory by NIH GM060992 and core resources funded by the Diabetes Endocrinology Research Center (grant DK32520), in the Wang laboratory by NIH GM070820, and in the Lo laboratory by NIH funding ZO1-HL005701 and U01-HL098180.

COMPETING INTERESTS

The authors declare no competing financial interests.

AUTHOR CONTRIBUTIONS

C.C. and C.W.L. collected and processed necropsy images, J.T.S. and G.J.P. immunostained kidney sections, D.F. immunostained and counted cilia in MEFs, C.H. and C.C. performed skeletal-prep staining, Q.Y. recovered the mutant, B.C., Q.Y. and B.L. identified the mutation, B.C. performed western blotting of HEK293 cells expressing FLAG-tagged Mks1, C.C. immunostained HEK293 cells and MEFs, G.J.P. transfected GFP-tagged *Mks1* constructs into IMCD kidney cells, C.C. performed scanning EM analysis, immunostained neural tube sections and performed in-situ hybridizations, T.T. performed western blotting with anti-Gli3 antibody on limb tissues, C.C. and B.W. performed Gli2 western blotting on neural tube tissues, C.C. performed Gli3 western blotting on neural tube tissues, R.F. carried out high-speed videomicroscopy to image nodal and trachea epithelia ciliary motion, C.C. and C.W.L. processed data and images, C.W.L. designed ENU screening and developed concept, C.W.L., C.C. and G.J.P. designed experiments, and C.C., G.J.P. and C.W.L. wrote the manuscript.

SUPPLEMENTARY MATERIAL

Supplementary material for this article is available at
http://dmm.biologists.org/lookup/suppl/doi:10.1242/dmm.006262/-/DC1

REFERENCES

Albrecht, U., Eichele, G., Helms, J. A. and Lu, H. C. (1997). *Molecular and Cellular Methods in Developmental Toxicology* (ed. G. P. Daston), pp. 23-48. New York: CRC Incorporated.

Baala, L., Audollent, S., Martinovic, J., Ozilou, C., Babron, M. C., Sivanandamoorthy, S., Saunier, S., Salomon, R., Gonzales, M., Rattenberry, E. et al. (2007). Pleiotropic effects of CEP290 (NPHP6) mutations extend to Meckel syndrome. *Am. J. Hum. Genet.* **81**, 170-179.

Berbari, N. F., O'Connor, A. K., Haycraft, C. J. and Yoder, B. K. (2009). The primary cilium as a complex signaling center. *Curr. Biol.* **19**, R526-R535.

Braithwaite, J. M. and Economides, D. L. (1995). First-trimester diagnosis of Meckel-Gruber syndrome by transabdominal sonography in a low-risk case. *Prenat. Diagn.* **15**, 1168-1170.

Brown, N. E. and Murcia, N. S. (2003). Delayed cystogenesis and increased ciliogenesis associated with the re-expression of polaris in Tg737 mutant mice. *Kidney Int.* **63**, 1220-1229.

Caspary, T., Larkins, C. E. and Anderson, K. V. (2007). The graded response to Sonic Hedgehog depends on cilia architecture. *Dev. Cell* **12**, 767-778.

Corbit, K. C., Shyer, A. E., Dowdle, W. E., Gaulden, J., Singla, V., Chen, M. H., Chuang, P. T. and Reiter, J. F. (2008). Kif3a constrains beta-catenin-dependent Wnt signalling through dual ciliary and non-ciliary mechanisms. *Nat. Cell Biol.* **10**, 70-76.

Dammermann, A., Pemble, H., Mitchell, B. J., McLeod, I., Yates, J. R., 3rd, Kintner, C., Desai, A. B. and Oegema, K. (2009). The hydrolethalus syndrome protein HYLS-1 links core centriole structure to cilia formation. *Genes Dev.* **23**, 2046-2059.

Dawe, H. R., Smith, U. M., Cullinane, A. R., Gerrelli, D., Cox, P., Badano, J. L., Blair-Reid, S., Sriram, N., Katsanis, N., Attie-Bitach, T. et al. (2007). The Meckel-Gruber Syndrome proteins MKS1 and meckelin interact and are required for primary cilium formation. *Hum. Mol. Genet.* **16**, 173-186.

Delous, M., Baala, L., Salomon, R., Laclef, C., Vierkotten, J., Tory, K., Golzio, C., Lacoste, T., Besse, L., Ozilou, C. et al. (2007). The ciliary gene RPGRIP1L is mutated in cerebello-oculo-renal syndrome (Joubert syndrome type B) and Meckel syndrome. *Nat. Genet.* **39**, 875-881.

Ding, Q., Motoyama, J., Gasca, S., Mo, R., Sasaki, H., Rossant, J. and Hui, C. C. (1998). Diminished Sonic hedgehog signaling and lack of floor plate differentiation in Gli2 mutant mice. *Development* **125**, 2533-2543.

Ding, X., Bishop, R. J., Herzlich, A. A., Patel, M. and Chan, C. C. (2009). Limbal stem cell deficiency arising from systemic chemotherapy with hydroxycarbamide. *Cornea* **28**, 221-223.

Eggenschwiler, J. T. and Anderson, K. V. (2007). Cilia and developmental signaling. *Annu. Rev. Cell Dev. Biol.* **23**, 345-373.

Ferrante, M. I., Zullo, A., Barra, A., Bimonte, S., Messaddeq, N., Studer, M., Dolle, P. and Franco, B. (2006). Oral-facial-digital type I protein is required for primary cilia formation and left-right axis specification. *Nat. Genet.* **38**, 112-117.

Fischer, E., Legue, E., Doyen, A., Nato, F., Nicolas, J. F., Torres, V., Yaniv, M. and Pontoglio, M. (2006). Defective planar cell polarity in polycystic kidney disease. *Nat. Genet.* **38**, 21-23.

Follit, J. A., San Agustin, J. T., Xu, F., Jonassen, J. A., Samtani, R., Lo, C. W. and Pazour, G. J. (2008). The Golgin GMAP210/TRIP11 anchors IFT20 to the Golgi complex. *PLoS Genet.* **4**, e1000315.

Francis, R. J., Chatterjee, B., Loges, N. T., Zentgraf, H., Omran, H. and Lo, C. W. (2009). Initiation and maturation of cilia-generated flow in newborn and postnatal mouse airway. *Am. J. Physiol.* **296**, L1067-L1075.

Fraser, F. C. and Lytwyn, A. (1981). Spectrum of anomalies in the Meckel syndrome, or: "Maybe there is a malformation syndrome with at least one constant anomaly". *Am. J. Med. Genet.* **9**, 67-73.

Gerdes, J. M. and Katsanis, N. (2008). Ciliary function and Wnt signal modulation. *Curr. Top. Dev. Biol.* **85**, 175-195.

Gerdes, J. M., Davis, E. E. and Katsanis, N. (2009). The vertebrate primary cilium in development, homeostasis, and disease. *Cell* **137**, 32-45.

Gorden, N. T., Arts, H. H., Parisi, M. A., Coene, K. L., Letteboer, S. J., van Beersum, S. E., Mans, D. A., Hikida, A., Eckert, M., Knutzen, D. et al. (2008). CC2D2A is mutated in Joubert syndrome and interacts with the ciliopathy-associated basal body protein CEP290. *Am. J. Hum. Genet.* **83**, 559-571.

Hashimoto, M., Shinohara, K., Wang, J., Ikeuchi, S., Yoshiba, S., Meno, C., Nonaka, S., Takada, S., Hatta, K., Wynshaw-Boris, A. et al. (2010). Planar polarization of node cells determines the rotational axis of node cilia. *Nat. Cell Biol.* **12**, 170-176.

Haycraft, C. J., Banizs, B., Aydin-Son, Y., Zhang, Q., Michaud, E. J. and Yoder, B. K. (2005). Gli2 and Gli3 localize to cilia and require the intraflagellar transport protein polaris for processing and function. *PLoS Genet.* **1**, e53.

Hirokawa, N., Tanaka, Y., Okada, Y. and Takeda, S. (2006). Nodal flow and the generation of left-right asymmetry. *Cell* **125**, 33-45.

Hooper, J. E. and Scott, M. P. (2005). Communicating with Hedgehogs. *Nat. Rev. Mol. Cell Biol.* **6**, 306-317.

Huangfu, D. and Anderson, K. V. (2005). Cilia and Hedgehog responsiveness in the mouse. *Proc. Natl. Acad. Sci. USA* **102**, 11325-11330.

Huangfu, D., Liu, A., Rakeman, A. S., Murcia, N. S., Niswander, L. and Anderson, K. V. (2003). Hedgehog signalling in the mouse requires intraflagellar transport proteins. *Nature* **426**, 83-87.

Ibanez-Tallon, I., Heintz, N. and Omran, H. (2003). To beat or not to beat: roles of cilia in development and disease. *Hum. Mol. Genet.* **12**, R27-R35.

Ickowicz, V., Eurin, D., Maugey-Laulom, B., Didier, F., Garel, C., Gubler, M. C., Laquerriere, A. and Avni, E. F. (2006). Meckel-Gruber syndrome: sonography and pathology. *Ultrasound Obstet. Gynecol.* **27**, 296-300.

Jonassen, J. A., San Agustin, J., Follit, J. A. and Pazour, G. J. (2008). Deletion of IFT20 in the mouse kidney causes misorientation of the mitotic spindle and cystic kidney disease. *J. Cell Biol.* **183**, 377-384.

Jones, C., Roper, V. C., Foucher, I., Qian, D., Banizs, B., Petit, C., Yoder, B. K. and Chen, P. (2008). Ciliary proteins link basal body polarization to planar cell polarity regulation. *Nat. Genet.* **40**, 69-77.

Katsanis, N. (2006). Ciliary proteins and exencephaly. *Nat. Genet.* **38**, 135-136.

Kelly, M. and Chen, P. (2007). Shaping the mammalian auditory sensory organ by the planar cell polarity pathway. *Int. J. Dev. Biol.* **51**, 535-547.

Kume, T., Deng, K. and Hogan, B. L. (2000). Murine forkhead/winged helix genes Foxc1 (Mf1) and Foxc2 (Mfh1) are required for the early organogenesis of the kidney and urinary tract. *Development* **127**, 1387-1395.

Kyttala, M., Tallila, J., Salonen, R., Kopra, O., Kohlschmidt, N., Paavola-Sakki, P., Peltonen, L. and Kestila, M. (2006). MKS1, encoding a component of the flagellar apparatus basal body proteome, is mutated in Meckel syndrome. *Nat. Genet.* **38**, 155-157.

Lancaster, M. A., Louie, C. M., Silhavy, J. L., Sintasath, L., Decambre, M., Nigam, S. K., Willert, K. and Gleeson, J. G. (2009). Impaired Wnt-beta-catenin signaling disrupts adult renal homeostasis and leads to cystic kidney ciliopathy. *Nat. Med.* **15**, 1046-1054.

Matise, M. P., Epstein, D. J., Park, H. L., Platt, K. A. and Joyner, A. L. (1998). Gli2 is required for induction of floor plate and adjacent cells, but not most ventral neurons in the mouse central nervous system. *Development* **125**, 2759-2770.

McGrath, J., Somlo, S., Makova, S., Tian, X. and Brueckner, M. (2003). Two populations of node monocilia initiate left-right asymmetry in the mouse. *Cell* **114**, 61-73.

McMahon, A. P., Ingham, P. W. and Tabin, C. J. (2003). Developmental roles and clinical significance of hedgehog signaling. *Curr. Top. Dev. Biol.* **53**, 1-114.

McNeill, H. (2009). Planar cell polarity and the kidney. *J. Am. Soc. Nephrol.* **20**, 2104-2111.

Mecke, S. and Passarge, E. (1971). Encephalocele, polycystic kidneys, and polydactyly as an autosomal recessive trait simulating certain other disorders: the Meckel syndrome. *Ann. Genet.* **14**, 97-103.

Miyazaki, Y., Oshima, K., Fogo, A., Hogan, B. L. and Ichikawa, I. (2000). Bone morphogenetic protein 4 regulates the budding site and elongation of the mouse ureter. *J. Clin. Invest.* **105**, 863-873.

Mo, R., Freer, A. M., Zinyk, D. L., Crackower, M. A., Michaud, J., Heng, H. H., Chik, K. W., Shi, X. M., Tsui, L. C., Cheng, S. H. et al. (1997). Specific and redundant functions of Gli2 and Gli3 zinc finger genes in skeletal patterning and development. *Development* **124**, 113-123.

Murcia, N. S., Richards, W. G., Yoder, B. K., Mucenski, M. L., Dunlap, J. R. and Woychik, R. P. (2000). The Oak Ridge Polycystic Kidney (orpk) disease gene is required for left-right axis determination. *Development* **127**, 2347-2355.

Nauli, S. M., Alenghat, F. J., Luo, Y., Williams, E., Vassilev, P., Li, X., Elia, A. E., Lu, W., Brown, E. M., Quinn, S. J. et al. (2003). Polycystins 1 and 2 mediate mechanosensation in the primary cilium of kidney cells. *Nat. Genet.* **33**, 129-137.

Neuhaus, I. M. and Beier, D. R. (1998). Efficient localization of mutations by interval haplotype analysis. *Mamm. Genome* **9**, 150-154.

Nyberg, D. A., Hallesy, D., Mahony, B. S., Hirsch, J. H., Luthy, D. A. and Hickok, D. (1990). Meckel-Gruber syndrome. Importance of prenatal diagnosis. *J. Ultrasound Med.* **9**, 691-696.

Okada, Y., Takeda, S., Tanaka, Y., Belmonte, J. C. and Hirokawa, N. (2005). Mechanism of nodal flow: a conserved symmetry breaking event in left-right axis determination. *Cell* **121**, 633-644.

Pan, Y., Bai, C. B., Joyner, A. L. and Wang, B. (2006). Sonic hedgehog signaling regulates Gli2 transcriptional activity by suppressing its processing and degradation. *Mol. Cell. Biol.* **26**, 3365-3377.

Pazour, G. J., Dickert, B. L., Vucica, Y., Seeley, E. S., Rosenbaum, J. L., Witman, G. B. and Cole, D. G. (2000). Chlamydomonas IFT88 and its mouse homologue, polycystic kidney disease gene tg737, are required for assembly of cilia and flagella. *J. Cell Biol.* **151**, 709-718.

Rohatgi, R., Milenkovic, L. and Scott, M. P. (2007). Patched1 regulates hedgehog signaling at the primary cilium. *Science* **317**, 372-376.

Roume, J., Genin, E., Cormier-Daire, V., Ma, H. W., Mehaye, B., Attie, T., Razavi-Encha, F., Fallet-Bianco, C., Buenerd, A., Clerget-Darpoux, F. et al. (1998). A gene for Meckel syndrome maps to chromosome 11q13. *Am. J. Hum. Genet.* **63**, 1095-1101.

Saadi-Kheddouci, S., Berrebi, D., Romagnolo, B., Cluzeaud, F., Peuchmaur, M., Kahn, A., Vandewalle, A. and Perret, C. (2001). Early development of polycystic kidney disease in transgenic mice expressing an activated mutant of the beta-catenin gene. *Oncogene* **20**, 5972-5981.

Salonen, R. (1984). The Meckel syndrome: clinicopathological findings in 67 patients. *Am. J. Med. Genet.* **18**, 671-689.

Salonen, R. and Paavola, P. (1998). Meckel syndrome. *J. Med. Genet.* **35**, 497-501.

Satir, P. and Christensen, S. T. (2007). Overview of structure and function of mammalian cilia. *Annu. Rev. Physiol.* **69**, 377-400.

Sepulveda, W., Sebire, N. J., Souka, A., Snijders, R. J. and Nicolaides, K. H. (1997). Diagnosis of the Meckel-Gruber syndrome at eleven to fourteen weeks' gestation. *Am. J. Obstet. Gynecol.* **176**, 316-319.

Sharma, N., Berbari, N. F. and Yoder, B. K. (2008). Ciliary dysfunction in developmental abnormalities and diseases. *Curr. Top. Dev. Biol.* **85**, 371-427.

Shen, Y., Leatherbury, L., Rosenthal, J., Yu, Q., Pappas, M. A., Wessels, A., Lucas, J., Siegfried, B., Chatterjee, B., Svenson, K. et al. (2005). Cardiovascular phenotyping of fetal mice by noninvasive high-frequency ultrasound facilitates recovery of ENU-induced mutations causing congenital cardiac and extracardiac defects. *Physiol. Genomics* **24**, 23-36.

Shiba, D., Yamaoka, Y., Hagiwara, H., Takamatsu, T., Hamada, H. and Yokoyama, T. (2009). Localization of Inv in a distinctive intraciliary compartment requires the C-terminal ninein-homolog-containing region. *J. Cell Sci.* **122**, 44-54.

Simons, M., Gloy, J., Ganner, A., Bullerkotte, A., Bashkurov, M., Kronig, C., Schermer, B., Benzing, T., Cabello, O. A., Jenny, A. et al. (2005). Inversin, the gene product mutated in nephronophthisis type II, functions as a molecular switch between Wnt signaling pathways. *Nat. Genet.* **37**, 537-543.

Smith, U. M., Consugar, M., Tee, L. J., McKee, B. M., Maina, E. N., Whelan, S., Morgan, N. V., Goranson, E., Gissen, P., Lilliquist, S. et al. (2006). The transmembrane protein meckelin (MKS3) is mutated in Meckel-Gruber syndrome and the wpk rat. *Nat. Genet.* **38**, 191-196.

Supp, D. M., Witte, D. P., Potter, S. S. and Brueckner, M. (1997). Mutation of an axonemal dynein affects left-right asymmetry in inversus viscerum mice. *Nature* **389**, 963-966.

Tallila, J., Jakkula, E., Peltonen, L., Salonen, R. and Kestila, M. (2008). Identification of CC2D2A as a Meckel syndrome gene adds an important piece to the ciliopathy puzzle. *Am. J. Hum. Genet.* **82**, 1361-1367.

Town, T., Breunig, J. J., Sarkisian, M. R., Spilianakis, C., Ayoub, A. E., Liu, X., Ferrandino, A. F., Gallagher, A. R., Li, M. O., Rakic, P. et al. (2008). The stumpy

gene is required for mammalian ciliogenesis. *Proc. Natl. Acad. Sci. USA* **105**, 2853-2858.

Tran, P. V., Haycraft, C. J., Besschetnova, T. Y., Turbe-Doan, A., Stottmann, R. W., Herron, B. J., Chesebro, A. L., Qiu, H., Scherz, P. J., Shah, J. V. et al. (2008). THM1 negatively modulates mouse sonic hedgehog signal transduction and affects retrograde intraflagellar transport in cilia. *Nat. Genet.* **40**, 403-410.

Vierkotten, J., Dildrop, R., Peters, T., Wang, B. and Ruther, U. (2007). Ftm is a novel basal body protein of cilia involved in Shh signalling. *Development* **134**, 2569-2577.

Wang, B., Fallon, J. F. and Beachy, P. A. (2000). Hedgehog-regulated processing of Gli3 produces an anterior/posterior repressor gradient in the developing vertebrate limb. *Cell* **100**, 423-434.

Weatherbee, S. D., Niswander, L. A. and Anderson, K. V. (2009). A mouse model for Meckel syndrome reveals Mks1 is required for ciliogenesis and Hedgehog signaling. *Hum. Mol. Genet.* **18**, 4565-4575.

Wheatley, D. N. (1982). *The Centriole, a Central Enigma of Cell Biology.* Amsterdam, New York, NY: Elsevier Biomedical Press.

Williams, C. L., Winkelbauer, M. E., Schafer, J. C., Michaud, E. J. and Yoder, B. K. (2008). Functional redundancy of the B9 proteins and nephrocystins in Caenorhabditis elegans ciliogenesis. *Mol. Biol. Cell* **19**, 2154-2168.

Wong, S. Y. and Reiter, J. F. (2008). The primary cilium at the crossroads of mammalian hedgehog signaling. *Curr. Top. Dev. Biol.* **85**, 225-260.

Yu, J., Carroll, T. J. and McMahon, A. P. (2002). Sonic hedgehog regulates proliferation and differentiation of mesenchymal cells in the mouse metanephric kidney. *Development* **129**, 5301-5312.

Yu, Q., Shen, Y., Chatterjee, B., Siegfried, B. H., Leatherbury, L., Rosenthal, J., Lucas, J. F., Wessels, A., Spurney, C. F., Wu, Y. J. et al. (2004). ENU induced mutations causing congenital cardiovascular anomalies. *Development* **131**, 6211-6223.

Zhang, Z., Alpert, D., Francis, R., Chatterjee, B., Yu, Q., Tansey, T., Sabol, S. L., Cui, C., Bai, Y., Koriabine, M. et al. (2009). Massively parallel sequencing identifies the gene Megf8 with ENU-induced mutation causing heterotaxy. *Proc. Natl. Acad. Sci. USA* **106**, 3219-3224.